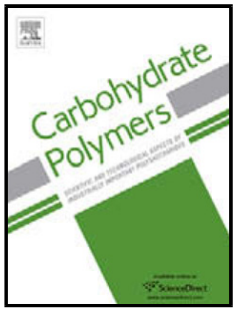

Title: Probing adhesion between nanoscale cellulose fibres using AFM lateral force spectroscopy: the effect of hemicelluloses on hydrogen bonding

Authors: Grace K. Dolan, Ben Cartwright, Mauricio R. Bonilla, Michael J. Gidley, Jason R. Stokes, Gleb E. Yakubov

PII: S0144-8617(18)31498-X
DOI: https://doi.org/10.1016/j.carbpol.2018.12.052
Reference: CARP 14406

To appear in:

Received date: 15 November 2018
Revised date: 17 December 2018
Accepted date: 17 December 2018

Please cite this article as: Dolan GK, Cartwright B, Bonilla MR, Gidley MJ, Stokes JR, Yakubov GE, Probing adhesion between nanoscale cellulose fibres using AFM lateral force spectroscopy: the effect of hemicelluloses on hydrogen bonding, *Carbohydrate Polymers* (2018), https://doi.org/10.1016/j.carbpol.2018.12.052

Probing adhesion between nanoscale cellulose fibres using AFM lateral force spectroscopy: the effect of hemicelluloses on hydrogen bonding

Grace K. Dolan[1,2], Ben Cartwright[2], Mauricio R. Bonilla[1,2‡], Michael J. Gidley[3], Jason R. Stokes[1,2], Gleb E. Yakubov[1,2⁎*]

[1]Australian Research Council Centre of Excellence in Plant Cell Walls, The University of Queensland, Brisbane, QLD 4072, Australia

[2]School of Chemical Engineering, The University of Queensland, Brisbane, QLD 4072, Australia

[3]Centre for Nutrition and Food Sciences, Queensland Alliance for Agriculture and Food Innovation, The University of Queensland, Brisbane, QLD 4072, Australia

⁎ Corresponding author's e-mail address: gleb.yakubov@uq.edu.au

Current address:
‡ IKERBASQUE, Basque Foundation of Science, 48011 Bilbao, Spain
⁎ Division of Food Sciences, School of Biosciences, University of Nottingham, Sutton Bonington Campus, Loughborough LE12 5RD, United Kingdom

Graphical abstract

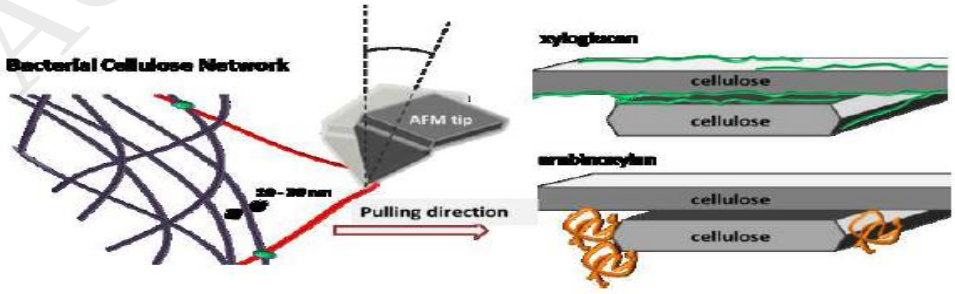

Highlights

- Developed an AFM technique to probe adhesion in cellulose-based networks.
- Characterized the nanoscale adhesion forces between cellulose fibres.
- Assessed the effect of xyloglucan and arabinoxylan on nano-scale adhesion forces.
- Provided insights into the effect of xyloglucan on cellulose-cellulose adhesion.

Abstract

Inter-fibre adhesion is a key contributing factor to the mechanical response and functionality of cellulose-based biomaterials. 'Dip-and-Drag' lateral force atomic force microscopy technique is used here to evaluate the influence of arabinoxylan and xyloglucan on interactions between nanoscale cellulose fibres within a hydrated network of bacterial cellulose. A cohesive zone model of the detachment event between two nano-fibres is used to interpret the experimental data and evaluate inter-fibre adhesion energy. The presence of xyloglucan or arabinoxylan is found to increase the adhesive energy by a factor of 4.3 and 1.3, respectively, which is consistent with these two hemicellulose polysaccharides having different specificity of hydrogen bonding with cellulose. Importantly, xyloglucan's ability to strengthen adhesion between cellulose nano-fibres supports emergent models of the primary plant cell walls (Park & Cosgrove, 2012b), which suggest that xyloglucan chains confined within cellulose-cellulose junctions play a key role in cell wall's mechanical response.

Keywords: cellulose; nanoscale; adhesion; hemicellulose; atomic force microscopy; hydrogen bonding.

1. Introduction

The remarkable combination of lightweight structure, load bearing capacity, and mechanical toughness of cellulose-based materials explains their ubiquitous utilisation in nature as a key structural component of the cell walls of plants and algae. The same set of physical properties alongside the inherent biocompatibility of cellulose-based materials make them an attractive and extremely versatile option for developing hydrogel materials and bio-mimetic systems for medical (de Oliveira Barud et al., 2016; Lv et al., 2016), pharmaceutical (Yang & Li, 2018) and food applications (Shi, Zhang, Phillips & Yang, 2014). Recent advances in cellulose-based biomaterials have been stimulated by new insights

gained from analysing the structure and mechanical properties of plant cell walls, which provided a deeper knowledge of cellulose fibre assembly and the role of non-cellulosic polymers in modulating mechanics of fibre networks.

Plant cell walls (PCW) exhibit a fine tuning of molecular and colloidal interactions between cellulose, hemicellulose polysaccharides and lignin that underpin material properties. A special class of PCWs is primary cell walls in which cell growth is permitted; these walls are highly deformable and typically contain no lignin. Within the primary PCW fibre network, cellulose is the main load-bearing component and hemicelluloses act as a water holding matrix (Dolan, Yakubov & Stokes, 2018). In addition, hemicelluloses play the role of cellulose deposition 'managers' influencing fibre orientation and association, and are responsible for tuning the microstructure of the cellulose sub-network (Johnson, Gidley, Bacic & Doblin, 2018). The strength of adhesion between cellulose fibres and between cellulose and the surrounding polymer matrix is a key determining factor of the network mechanics. Despite this pivotal importance of inter-fibre links, no direct measurements of the adhesive forces between nanoscale cellulose fibres have yet been reported. Furthermore, there is little known about the mechanistic details of the role of hemicelluloses in the structure and energy of adhesive contacts between cellulose fibres. Bridging this knowledge gap has fundamental importance for understanding the structure and mechanics of PCWs that underpin key processes controlling cell growth and morphogenesis (Cosgrove, 2014). In addition, the ability to manipulate adhesion between nano-fibres is instrumental for enabling biomimetic engineering of fibre-based networks (Chen et al., 2017; Lopez-Sanchez et al., 2017).

The properties of fibre-fibre contacts in PCWs arise from hydrogen bonding and van-der-Waals interactions between cellulose microfibrils as well as between hemicellulose polysaccharides and the surface layer of cellulose microfibrils (Cosgrove, 2014; Park & Cosgrove, 2012b; Zhang, Zheng & Cosgrove, 2016). The surface of plant or bacterial cellulose microfibrils is described as having a paracrystalline structure that forms a shell around the crystalline domain in the core of the fibril (Fernandes et al., 2011; Kulasinski, Keten, Churakov, Derome & Carmeliet, 2014). Such a hierarchical core-shell structure has been corroborated based on small angle scattering techniques, XRD, and SEM (Martinez-Sanz, Gidley & Gilbert, 2015). The paracrystalline state has intermediate mechanical properties between crystalline (high modulus) and amorphous (low modulus) phases. The partially ordered structure of the paracrystalline surface layer is thought to permit an association between the crystalline cellulose core and hemicellulose in the cell wall (Kulasinski, Keten, Churakov, Derome & Carmeliet, 2014). This model of architecture and assembly of cellulose networks is largely based on direct visualisation experiments (Kafle et al., 2014; Zhang, Mahgsoudy-Louyeh, Tittmann & Cosgrove, 2014), tensile mechanical testing on native and/or enzyme treated macroscopic substrates (Gu & Catchmark, 2014; Park & Cosgrove, 2012a; Whitney, Gothard, Mitchell & Gidley, 1999), as well as *in silico* modelling (Oehme,

Doblin, Wagner, Bacic, Downton & Gidley, 2015; Oehme, Downton, Doblin, Wagner, Gidley & Bacic, 2015).

The most abundant primary cell wall hemicelluloses across plant species are xyloglucan (XG) and arabinoxylan (AX). XG has a cellulosic backbone extensively decorated with carbohydrate sidechains, and binds to the cellulose surface predominantly due to hydrogen bonding (Finkenstadt, Hendrixson & Millane, 1995; Hanus & Mazeau, 2006; Keegstra, Talmadge, Bauer & Albershe.P, 1973; Whitney, Brigham, Darke, Reid & Gidley, 1995; Zykwinska, Ralet, Garnier & Thibault, 2005). More recently, Park and Cosgrove (2012b) established that XG-cellulose interaction may be more complex, and involve polymer entanglement between XG and amorphous cellulose chains on the fibril surface (Park & Cosgrove, 2012b; Zhao & Kwon, 2011). In addition, a number of other mechanisms have been proposed for XG-cellulose interactions, including: physical entrapment of XG molecules inside the cellulose microfibril during synthesis (Baba, Sone, Misaki & Hayashi, 1994; Park & Cosgrove, 2012b); covalent bonding of cellulose with XG via a transglycosylation reaction (Hrmova, Farkas, Lahnstein & Fincher, 2007); and lateral non-covalent bonding by a single XG layer mediating adhesion between adjacent microfibrils (Park & Cosgrove, 2012b). In contrast, AX is suggested to form non-specific associations between cellulose fibres (Martinez-Sanz, Mikkelsen, Flanagan, Gidley & Gilbert, 2017; Mikkelsen, Flanagan, Wilson, Bacic & Gidley, 2015; Mikkelsen & Gidley, 2011). This is consistent with a xylan backbone that is less structurally compatible with cellulose than XG. *In vitro* cellulose binding experiments on the walls of barley aleurone cells (containing 85% arabinoxylan) suggest non-covalent bonds between the AX chains themselves and with cellulose fibres (McNeil, Albersheim, Taiz & Jones, 1975).

Currently, the most reliable information regarding inter-fibre adhesion is inferred from the analysis of macroscopic mechanical properties of cellulose networks. The mechanical properties of bacterial cellulose (BC) and composite hydrogels (with AX and XG) have been probed using small amplitude oscillatory shear (SAOS) rheology tests and large deformation uniaxial tensile testing (Whitney, Gothard, Mitchell & Gidley, 1999), and equi-biaxial tension (Chanliaud, Burrows, Jeronimidis & Gidley, 2002). In addition, the poroviscoelasticiy of cellulose composite gels has been probed using a combined compression-SAOS test procedure (Lopez-Sanchez et al., 2017; Lopez-Sanchez et al., 2016; Lopez-Sanchez, Rincon, Wang, Brulhart, Stokes & Gidley, 2014). From these mechanical tests, the modulus of cellulose hydrogels and cellulose composites are measured to be in the range from 0.1 to 1 MPa (Chanliaud, Burrows, Jeronimidis & Gidley, 2002; Lopez-Sanchez, Rincon, Wang, Brulhart, Stokes & Gidley, 2014; Whitney, Gothard, Mitchell & Gidley, 1999). The mechanical properties of fibre networks are, however, vastly different to individual cellulose fibres; the Young's modulus evaluated using an AFM-based three-point bending test of a suspended BC fibre was estimated to be of the order of 100 GPa (Guhados, Wan & Hutter, 2005). From these multi-scale measurements, and based on fibre network models, it is implicit that the mechanical properties of cellulose-based composites are

largely driven by interactions between cellulose fibres and matrix polymers that control the fibre deposition and orientation (Bonilla, Lopez-Sanchez, Gidley & Stokes, 2016; Gartaula et al., 2018).

The surface forces between model cellulose surfaces and cellulose fibre aggregates have been studied previously using AFM. For example, AFM imaging of onion epidermis shows that the cellulose microfibrils come into close proximity with one another (Zhang, Mahgsoudy-Louyeh, Tittmann & Cosgrove, 2014). However, due to inter-fibre separations being of the order of the width of a molecule, deducing the nature of interaction between cellulose fibres based on microscopy data alone presents a significant challenge. Thus, AFM-based force spectroscopy has been utilised for direct measurement of the friction and adhesion forces between model cellulose surfaces including pulp fibres (cellulose fibre aggregates ~10µm) (Andersson & Rasmuson, 1997; Huang, Li & Kulachenko, 2009), spherical cellulose particles (Carambassis & Rutland, 1999; Notley, Eriksson, Wagberg, Beck & Gray, 2006; Stiernstedt, Brumer, Zhou, Teeri & Rutland, 2006), and cellulose thin films (Nigmatullin, Lovitt, Wright, Linder, Nakari-Setala & Gama, 2004; Notley, Eriksson, Wagberg, Beck & Gray, 2006; Stiernstedt, Nordgren, Wagberg, Brumer, Gray & Rutland, 2006; Zauscher & Klingenberg, 2001). Despite these advances, our knowledge of cellulose fibre friction and adhesion is confined to large aggregates of cellulose fibres which are not representative of interactions between individual cellulose fibres (and nano-scale fibre bundles) that are typically found in primary plant cell walls and BC hydrogels (diameter $\sim 5-100$ nm) (Martinez-Sanz, Gidley & Gilbert, 2016; Martinez-Sanz, Lopez-Sanchez, Gidley & Gilbert, 2015).

In this work we aim to probe the interactive forces between nanoscale cellulose fibres and explore the effect of non-cellulosic components (arabinoxylan and xyloglucan) on inter-fibre adhesion (Dolan, 2017). To enable such nano-scale characterisation, we adapted and further advanced our recently developed dip-and-drag lateral force spectroscopy (DnD-LFS) technique (Dolan et al., 2016), which uses an AFM cantilever tip to pull fibres out of a network and measure forces associated with detachment events at fibre contacts. Building on previous developments (Lopez-Sanchez, Cersosimo, Wang, Flanagan, Stokes & Gidley, 2015; Martinez-Sanz, Mikkelsen, Flanagan, Gidley & Gilbert, 2017; Whitney, Gothard, Mitchell & Gidley, 1999), BC networks are used as a model system and are self-assembled to give a random distribution of fibre orientations and contact configurations. Whilst BC's network density and fibre alignment may differ from other types of cellulose networks such as PCWs, we expect that the physical nature of interactions between cellulose fibres and hemicelluloses probed using DND-LFS technique can uncover general mechanisms that underpin the impact of adhesive forces on the mechanical properties of cellulose network assemblies including PCWs.

2. Experimental Section

2.1. Cellulose micro-gel preparation

The method for producing pure BC networks and composites involves fermenting *Gluconacetobacter xylinus* in Hestin Schramm (HS) liquid medium followed from Mikkelsen and Gidley (2011). A frozen strain of *Gluconacetobacter xylinus* (ATCC 53524 American Type Culture Collection, Manassas, VA) stored at -80^{0}C is revived by incubating on HS agar medium at 30^{0}C for 48 hours. The resulting bacterial colonies are subsequently transferred to liquid HS medium, pH 5 (adjusted with 0.1M HCL), with 50 % (w/v) glucose solution to be incubated under static conditions for a further 48 hours. The cellulose matrix that forms on the surface of the medium contains trapped bacteria and an orbital platform shaker (KS 260 IKA-Werke, Staufen, Germany) is used at 350rpm for 5 min to dislodge them into the liquid medium that is subsequently used as a primary inoculum.

To produce cellulose-xyloglucan (CXG) and cellulose-arabinoxylan composites, a 1% solution of xyloglucan (tamarind xyloglucan, Lot 100402, Megazyme, Bray, Ireland) or arabinoxylan (medium viscosity wheat arabinoxylan, Lot 40302a, Megazyme, Bray, Ireland) in deionised water was mixed under sterile conditions with double concentrated HS medium (1:1) before inoculation. The concentration of hemicelluloses was 0.5% w/v as established in the previous work (Lopez-Sanchez, Cersosimo, Wang, Flanagan, Stokes & Gidley, 2015; Martinez-Sanz, Mikkelsen, Flanagan, Gidley & Gilbert, 2017; Mikkelsen, Flanagan, Wilson, Bacic & Gidley, 2015; Whitney, Gothard, Mitchell & Gidley, 1999).

Micro-gel disks are grown within the confined geometries of a polydimethylsiloxane (PDMS) mould microarray of 50 micron cylindrical wells as shown in Figure 1A (Yakubov et al., 2016). Primary inoculum (with or without hemicelluloses) is pipetted onto the surface of the plasma treated (hydrophilic) PDMS microarray to enable inoculum to spread and bacteria to sediment inside the individual wells. The surface of the microarray is blotted to remove excess liquid medium allowing micro-gels to grow as a thin layer on the surface of the confined micro-wells. The micro-gels are harvested after 48 hours incubation under static conditions by washing the surface of the microarray with ice cold water. The assessment of composition was based on the contents of individual sugars analysed using a GC-MS technique and a high polarity BPX70 column (Thermo Fisher Scientific, Australia) as reported previously (Lopez-Sanchez, Cersosimo, Wang, Flanagan, Stokes & Gidley, 2015). The estimated content of XG and AX in the corresponding composites was ~30 wt% and ~50 wt%, respectively.

Upon harvesting, the microarray with micro-gels is placed face down onto a plasma-treated glass substrate and the PDMS mould is peeled off after approximately 1 hour, leaving the micro-gels deposited on the glass surface. In a JPK Nanowizard II AFM mounted on an inverted optical microscope (JPK Instruments, Germany) using a cantilever and a 5-minute curing epoxy resin (UHU GmbH & Co. KG, Germany) (equal parts base and curing

agent), the micro-gels are glued to the surface at two opposite edges of the gel. Once glued, the micro-gels where washed with water (resistivity 18.2 MΩ·cm, Sartorius) to remove any weakly bound polymers. While in a wetted state, the substrate with the attached micro-gels was mounted on an AFM stage, and water was added by pipetting ~ 1 mL around the glass cantilever holder.

2.2. Imaging and Lateral Force Microscopy using manipulation control

High resolution images for characterisation of the cellulose network were obtained from a Cypher AFM (Asylum Research, Oxford Instruments, CA) with NSC/CSC Si tips (R ~ 10 nm) from Mikromasch (Nano World AG, Germany).

The lateral force measurements were performed using the JPK Nanowizard II AFM mounted on an inverted optical microscope (JPK Instruments, Germany) and equipped with a CellHesion® module. The AFM was loaded with a stiff cantilever (HQ:NSC35/Cr-Au BS, Cantilever A) from Mikromasch (Nano World AG, Germany). First, the hydrogels were imaged in intermittent contact mode in air. The imaging is performed at a scan rate of 2 Hz for a 60 x 60 µm scan size with 1024 x 1024 pixels. The set point and drive amplitudes are around 1 V and the drive frequency is around 200 kHz. Using the same cantilever, lateral force measurements are taken with a set point vertical deflection of 3V and the cantilever travel speed of 0.3 µm/s. Using manipulation control in contact mode, a cantilever path is traced over the image that was collected. A cantilever of high stiffness is used so that a high lateral force can be applied for separating fibre contact points. In order to hook onto the loose fibre loops around the edge of the micropellicle, the cantilever is engaged with the substrate several microns outside of the identified edge and dragged under fixed set point away from the micropellicle. Then the cantilever is lifted (disengaged) from the surface and moved (without touching the substrate) to the starting point of the subsequent trace which is incrementally closer to the edge of the micropellicle. This “dip-and drag” procedure is repeated several times until the first peaks in the lateral deflection curve are observed.

In order to ensure the tip is always in contact with the substrate, the normal load is set at c.a. 300nN. Such a high value of normal load ensured that the friction baseline, between tip and substrate remains constant so that changes in the lateral deflection can be confidently attributed to the detachment at the fibre contact points. The cantilever height is monitored to ensure that there is no significant change which would indicate the cantilever is lifting off the substrate and moving over fibres in the network, or otherwise indicating surface topography. The lateral deflection data is then recorded as a profile of lateral force versus cantilever travel distance.

The vertical spring constant is determined using the built-in heterodyne calibration procedure on the JPK AFM and the vertical cantilever sensitivity is measured from the slope of a vertical force-distance curve during retraction of the cantilever from a glass substrate. For lateral calibration of the cantilevers the Torsional Sader Method (Green, Lioe, Cleveland, Proksch, Mulvaney & Sader, 2004) is used to find the torsional spring constant, and the

lateral sensitivity is calculated using a non-contact calibration procedure (Wagner, Cheng & Vezenov, 2011). For a few cantilevers the reference cantilever method was applied (Yakubov, Macakova, Wilson, Windust & Stokes, 2015) and deviations did not exceed ~30%.

3 Development of Dip-and-Drag Lateral Force Spectroscopy (DnD-LFS) Technique for Probing Adhesive Contacts between Cellulose Fibres

3.1. Microstructure and DnD-LFS on BC hydrogels

The structure of cellulose fibres synthesised by *Gluconacetobacter xylinus* is hierarchical. First, the synthesised cellulose chains are extruded out of the pores in the bacteria's plasma membrane; these cellulose chains then assemble into microfibrils with a diameter of ca. 2-4 nm (Iguchi, Yamanaka et al. 2000). Subsequently, microfibrils aggregate into ribbon-shaped bundles with dimensions of the order of tens of nanometres. *G. xylinus* is used to produce sub-micrometre thin disk-shaped micropellicles of cellulose as shown in Figure 1A, which are utilised for DnD-LFS measurements. The vertical dimension of the fabricated micropellicles is smaller than the height of the AFM tip, which enables the tip to penetrate through the network and form a hard-wall contact with the glass substrate underneath. This hard-wall contact gives a baseline force during the DnD-LFS experiments. The morphologies of BC ribbons and fibre contacts are shown in Figure 1B and 1C. The cross-sectional analysis of the ribbon-shaped microfibril bundle (Figure 1C) is presented in Supplementary Figure S1; the estimated width of microfibrils is ~5 nm and the average width of the bundle is $D_B = 48 \pm 20$ nm (calculated using a MATLAB-based image analysis package), which suggests that each bundle is an assembly of ca. $5 - 20$ elementary fibrils. These dimensions and morphology are in broad agreement with observations on PCWs derived from onion (*Allium cepa*) epidermis by Zhang et al. (Zhang, Mahgsoudy-Louyeh, Tittmann & Cosgrove, 2014) and Kafle et al. (Kafle et al., 2014). They are also consistent with observations by Martinez-Sanz et al. (Martinez-Sanz, Gidley & Gilbert, 2016) that indicate that microfibril dimensions are very similar between bacteria and plants' primary walls, but bacterial microfibrils exhibit much greater degree of association.

The DnD-LFS technique, originally developed to probe adhesion between electrospun fibres (Dolan et al., 2016), has been advanced to make it applicable for probing inter-fibre adhesion in the BC systems. First, we have performed *in-situ* imaging of BC hydrogels and identify protruding fibre loops around the edge of the micropellicle. Then the AFM tip was positioned in the open space inside the loop and dragged away from the pellicle's edge, thus pulling the fibres away from the network, as depicted by the arrow in Figure 2A. The recorded lateral force-distance curves, an example of which is shown in Figure 2B, feature force peaks that consistently rise above the baseline. Following the methods established in our previous work (Dolan et al., 2016), the observed sharp increase

in force (above the baseline) is attributed to the AFM tip engaging with a cellulose fibre and dragging it until the latter is in tension[a]. This is followed by a detachment event at a fibre contact point (Dolan et al., 2016), when the fibre being pulled by the AFM tip is no longer in tension, which results in the cantilever deflection signal returning back to the baseline. For very low density networks, the friction force baseline (flat baseline) is anticipated to reflect the friction force between the glass substrate and the AFM tip. For dense systems, it is anticipated that the baseline force is also a function of the network mechanics and thus increases steadily with lateral distance. To make DnD-LFS technique suitable for BC, we have developed a signal processing algorithm and implemented it in MATLAB (see Supplementary Information for detailed description of the method). The algorithm identifies the cantilever deflection peaks directly from the experimental lateral force-distance spectra, and parameters such as the peak height, *h*, and the initial linear slope, *s*, are evaluated. The initial linear slope is determined by a linear fit of the ascending part of the force-distance curve prior to each peak as illustrated in Figure 2B. By analysing multiple force-distance curves recorded on at least 10 different micropellicles, the ensemble data is collected and used to construct the resulting distributions of parameters *h* and *s*.

A

[a] There is a chance that the cantilever engages several fibres at once. This scenario, however, accounts only for the second order correction to the measured pull-off forces as elaborated in (Dolan et al., 2016).

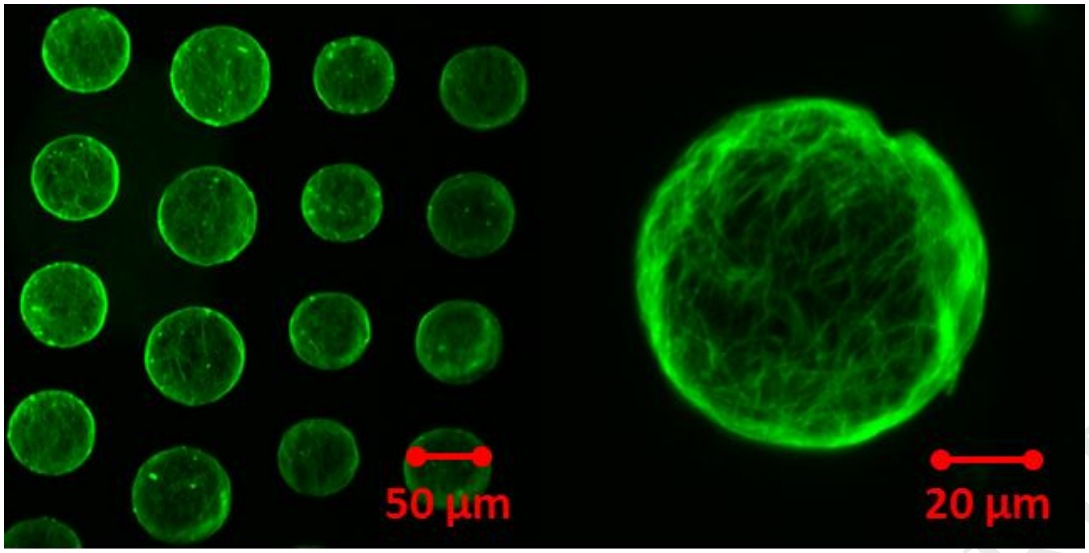

A

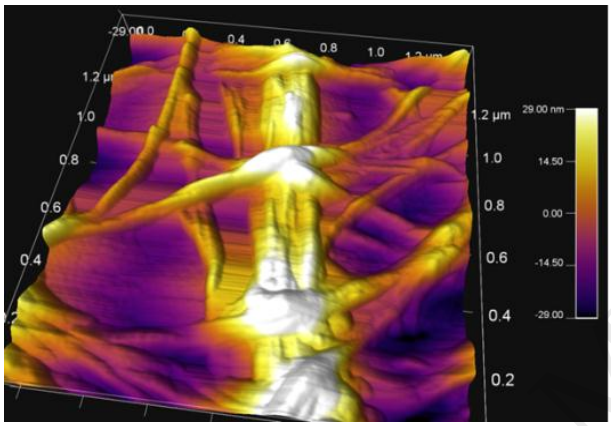

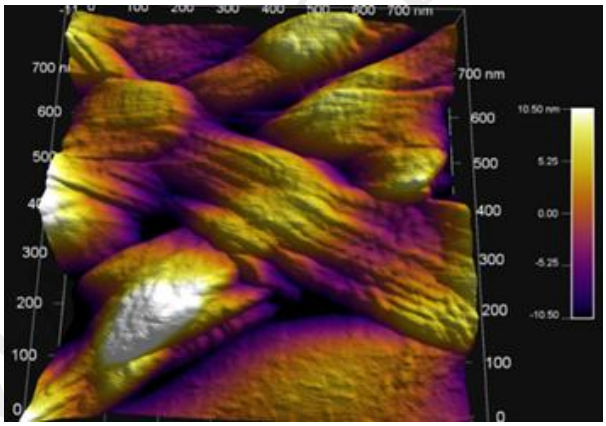

Figure 1. (A) Confocal scanning laser microscopy of BC pellicles grown inside an array of PDMS micro-wells. (B) AFM image of an air-dried cellulose network showing overall architecture. (C) Close-up AFM image of critical point dried cellulose network showing the ribbon structure of individual cellulose fibres and contact points. For (B) and (C) the colour scale on the left hand side is the vertical dimension of the topography in nm.

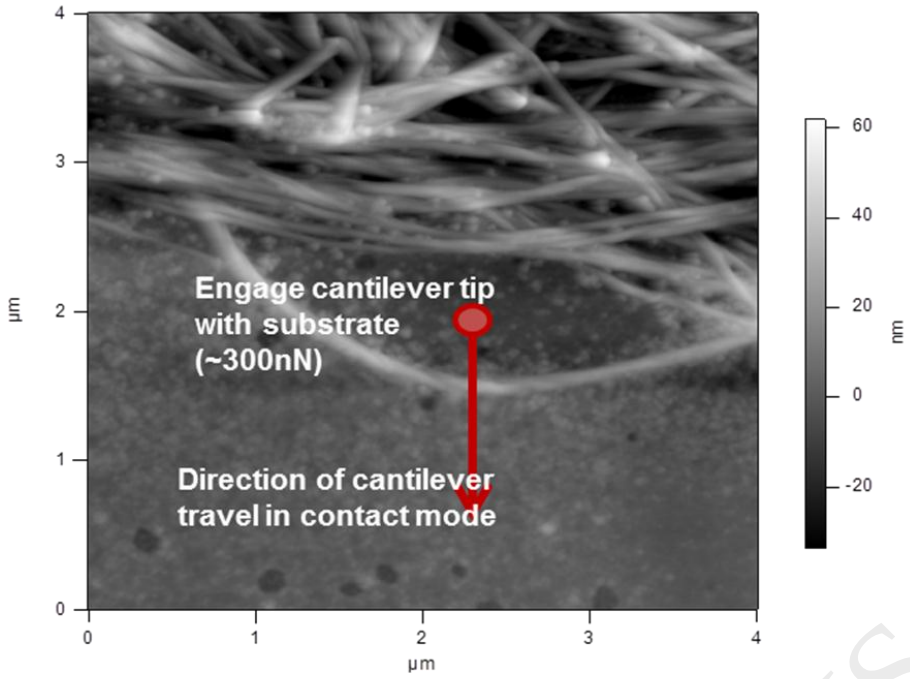

B

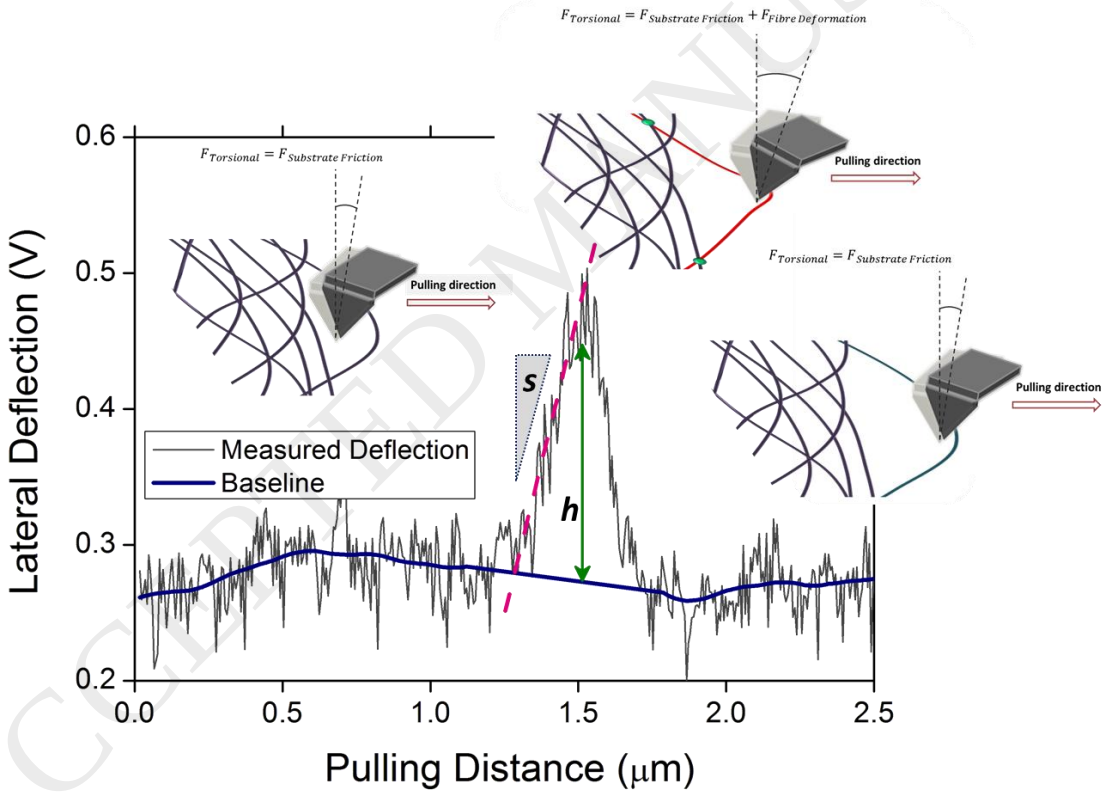

Figure 2. (A) AFM image of the edge of cellulose network showing a loose fibre loop that is pulled with the AFM tip. The arrow represents the desired path of the AFM tip, where it engages with the glass substrate at a vertical force of 300 nN and is then dragged outward from the network to bring the fibre into tension and drive a fibre detachment event. (B) Lateral force-distance curve showing a typical peak that is representative of a detachment event at a fibre contact point.

3.2. Simulating fibre-fibre detachment events

To assist in interpreting DnD-LFS results, a force balance across a section of a hypothetical network during a pulling experiment is considered, as illustrated in Figure 3. In order for a detachment event to occur, the force applied directly at a contact must be greater than the adhesive force between fibres. The AFM tip applies a force directly to the fibre that it is in contact with, and this force is divided between several fibres as one moves further into the network. For example, the 7 fibres at the bottom of the diagram experience approximately a seventh of the pulling force applied to the single fibre at the top system boundary. Thus, if the adhesive forces at all fibre contacts are from the same distribution, fibre detachment is most likely to occur at the first contact (see the circled contact in Figure 3) because it experiences the largest direct pulling force. In Figure 3, the pull-off force at the circled contact is assumed to be equal to the pulling force measured by the AFM tip at the point of detachment.

In order to simulate the scenario portrayed in Figure 3A, a simplified model is implemented in Comsol™ Multiphysics using the beam mechanics interface. The model setup is depicted in Figure 3B. Contacts 1 and 2 in Figure 3B are assumed to be fixed in the simulation. The cross-section of the fibrils is assumed to be rectangular (30 nm width × 15 nm height) and the fibril modulus is taken as 78 GPa (Guhados, Wan & Hutter, 2005). The contact is modelled as a collection of ten springs separated from each other by 1 nm; each spring has an equilibrium length, δ. The mechanics of the contact is set to follow a simplified cohesive zone model (CZM) structure (Park & Paulino, 2011), with the contact strength (or equivalently the modulus), *K*, following eq 1.

$$K = K_0 H(\varepsilon_c - \varepsilon) + K_0 e^{-\alpha(\varepsilon - \varepsilon_c)} H(\varepsilon - \varepsilon_c) \quad (1)$$

K_0 is the contact strength of unstretched springs, ε is contact strain, ε_c is the critical contact strain, and *H*(x) is the Heaviside function which takes the value of zero for $x < 0$ and unity for $x \geq 0$. Hence, the contact springs weaken exponentially when $\varepsilon > \varepsilon_c$. Since we examine the pull-off force (i.e. where $K = K_0$) and not the detachment length, the value of the decay constant α can be set arbitrarily and does not require further refinement; in all simulations the α was fixed at 15 for optimum numerical stability. This formalism is a slight departure from the usual CZM, which assumes a finite detachment displacement. For the present system, where fibre contacts are highly variable and dependent on the type of polymer (AX or XG), incorporating a finite detachment displacement is ambiguous as it cannot be extracted from the experimental data.

A

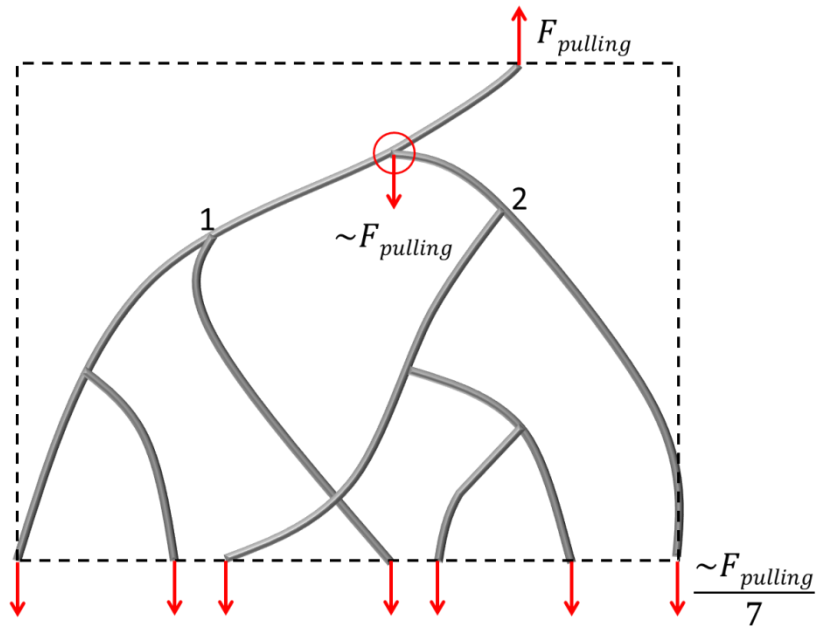

B

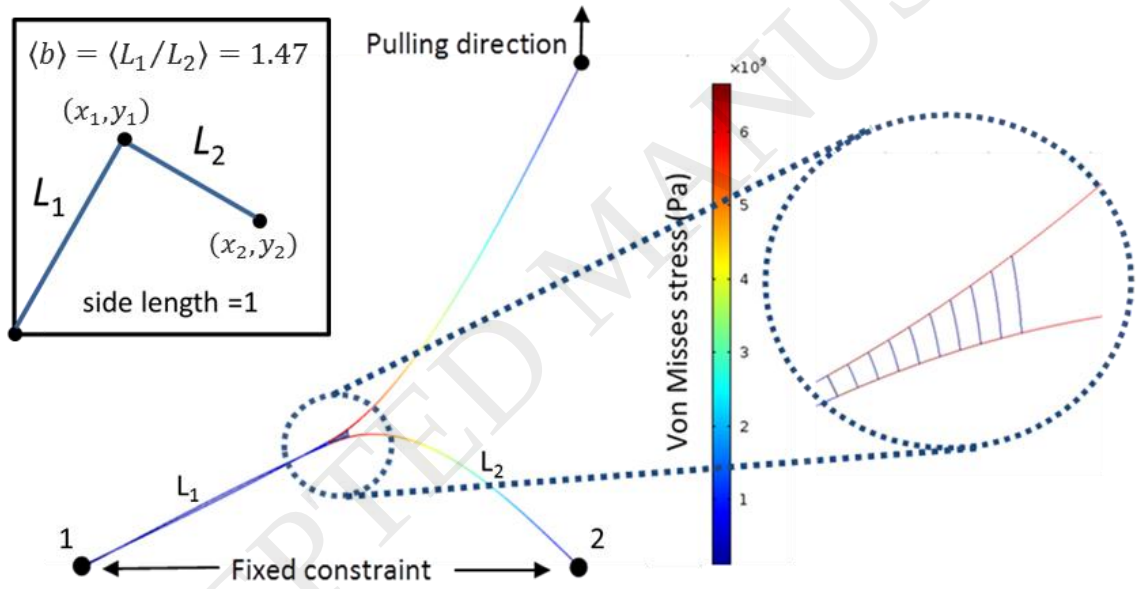

Figure 3. (A) Force balance across a section of the fibre network to illustrate that the pulling force recorded by the AFM tip is a good estimate of the force acting at the fibre-fibre contact closest to the pulling arm (encircled). The dashed line marks the system boundary over which the force balance is applied. (B) Simplified setup of the system depicted in (A) implemented in Comsol™ Multiphysics. Due to large aspect ratio of cellulose fibres they can be modelled as ideal beams. The adhesive contact is modelled as a collection of beams that soften when a critical strain, ε_c, is reached. Contacts 1 and 2 in are assumed to be fixed. (Inset) The sketch of the probability argument used to estimate the ensemble average value of the structural factor $b = L_1/L_2$.

Parametric sweeps are performed over K_0, ε_c, and the ratio between beam lengths ($b = L_1/L_2$). Some sample curves from the parametric sweeps at constant $\varepsilon_c = 0.40$ are presented in Supplementary Figure S2. The simulated pulling force increases linearly with pulling distance until a peak force is reached, beyond which the pulling force decreases as the contact strength decays and the fibres are separated. The peak pulling force is equivalent to the experimentally measured peak heights and is taken as the pull-off force between fibres under the specific conditions of K_0, ε_c, and b. When comparing the respective force-distance curves generated keeping K_0 and ε_c constant and varying b (see pairs of curves with open and closed symbols in Supplementary Figure S2), it is observed that b **does** change the initial (pre-maximum) force gradient (∇F_{CZM}) but **does not** affect the pull-off force. This result is fundamentally important because it confirms that, on average, the pull-off force is independent of the geometric configuration of the fibre network and the pulling geometry (e.g. pulling angle etc.).

We, however, note that the pre-maximum force gradient (∇F_{CZM}) does depend on both network mechanics as well as 'spring action' of contacts, and therefore the values of the slope extracted from experimental force spectra (s) are not explicitly related to ∇F_{CZM}. In order to estimate the contribution of network mechanics and enable comparison of experimental values of s with predictions of CZM model, we have mapped the function

$$\nabla F_{\mathrm{CZM}} = f(K_0, b) \tag{2}$$

Supplementary Figure S3 presents a 3-D plot of the functions in eq 2, and the equation of the best fits to the surface is given in eq 3.

$$\nabla F_{\mathrm{CZM}} = 1[N/m] \cdot exp\big[-8.59839 - 0.08275 \cdot (\ln K_0)^2 + 1.31794 \cdot \ln K_0 + 3.63849b - 4.81016 \cdot \sqrt{b} \cdot \ln b\big] \tag{3}$$

The expression for ∇F_{CZM} (eq 2) is a function of two parameters: K_0 and b. First, we estimate the contact strength, K_0, which is expected to be directly proportional to the experimental values of the pull-off force. The size of interacting cellulose fibres is of the order of 5 – 50 nm, while cellulose elastic modulus is estimated to be approximately 78 GPa (Guhados, Wan & Hutter, 2005). Using these values, we can estimate the critical crack length, using the expression derived by Carbone and Pierro (2013):

$$a_c = \tfrac{1}{2}\pi E \frac{\delta^2}{\Delta\gamma} \tag{4},$$

E is elastic modulus, δ is the distance between interacting surfaces, and $\Delta\gamma$ is adhesion energy per unit area. For contacts bound by van-der-Waals forces, we can assume δ = 1 nm and the value of Hamaker constant for cellulose determined by Notley et al. (Notley, Pettersson & Wågberg, 2004), $A_H = 3.5 \cdot 10^{-21}$ J, which yields $\Delta\gamma = A_{\mathrm{H}}/(12\pi\delta^2) \approx 0.1$ mJ/m^2. For this scenario one obtains $a_c \approx 1300$ μm, which is disproportionally large compared to

microfibre or bundle dimension. Alternatively, we evaluate a scenario where contacts are held by hydrogen bonding. In this case, $\Delta\gamma$ can be estimated assuming the energy of hydrogen bonding ($E_{H\text{-}b}$) in water is ~ 6.6 kJ/mol as obtained by Sheu et al. (Sheu, Yang, Selzle & Schlag, 2003). The density of hydrogen bonding per unit area can be evaluated from the distance between layers (d_l) along the polymerisation axis of cellulose microfibrils reported to be ~ 4.5 Å based on X-ray diffraction data (Martinez-Sanz, Mikkelsen, Flanagan, Gidley & Gilbert, 2016; Martinez-Sanz et al., 2016) and molecular dynamics models (Oehme, Doblin, Wagner, Bacic, Downton & Gidley, 2015; Oehme, Downton, Doblin, Wagner, Gidley & Bacic, 2015). Hence the approximate area per single hydrogen bond within the contact is $\propto d_l^2 \approx 20$ Å^2. Using these values, one obtains $\Delta\gamma \sim {E_{H-b}}/{(N_A d_l^2)} \approx 55$ mJ/m^2 (here, N_A is Avogadro's number). For the case of cellulose microfibrils interacting via hydrogen bonding, the distance between interacting surfaces, δ, includes a layer of adsorbed water (Raviv, Laurat & Klein, 2001). Hence, we estimate δ to be ca. 0.3 nm, which is of the order of the thickness of a water monolayer. For this scenario we obtain $a_c \approx 200$ nm, which is comparable with the upper bound for the width of a bundle, $D_B \sim 100$ nm. Therefore we conclude that $D_B/a_c \leq 1$, and, consequently, we determine that the pull-off process follows the decohesion mechanism (Carbone & Pierro, 2013), whereby:

$$K_0 = \frac{\Delta\gamma}{\delta} = \frac{F_{\text{pull-off}}}{D_B^2} \tag{5}$$

A crude estimate based on hydrogen bonding scenario ($\Delta\gamma$ = 55 mJ/m^2, δ = 0.3 nm) leads to the value of $K_0 \approx 180$ MPa. The postulated decohesion mechanism associated with reaching a critical contact stress implies that contributions from ε_c in the CZM model described in eq 1 are small and can be neglected.

The next step of examining eq 2 is the evaluation of parameter b. We estimate b based on a simple geometric argument; let us consider a problem shown in the inset of Figure 3B whereby $1/b$ is a ratio of an average distance between two random points within a unit square (L_2) to an average distance between either of the two points and the vertices of the square (L_1). Based on geometric probability of the configuration considered in Figure 3B, the basic calculus problem[b] leads to the expression for the average value of $\langle b \rangle$ shown in eq 6. In eq 6 we assume two points with coordinates $[x_1,y_1]$ and $[x_2,y_2]$, and the respective distances are $x = |x_1 - x_2|$ and $y = |y_1 - y_2|$. Using the estimated values of $\langle b \rangle \approx 1.47$ and $K_0 \approx 180$ MPa, we evaluate $\nabla F_{\text{CZM}} \approx 0.4$ N/m.

$$\langle b \rangle = \left\langle {L_1}/{L_2} \right\rangle = \left(\frac{4\int_0^1 \sqrt{x^2+y^2}(1-x)(1-y)dxdy}{\int_0^1 \sqrt{x^2+y^2}dxdy} \right)^{-1} = \left(1 - \frac{4\sqrt{2}-2}{5(\sqrt{2}+\ln(1+\sqrt{2}))} \right)^{-1} \approx 1.47 \tag{6}$$

[b] A popular reference to an analogous problem can be found on the MathWorks blog by Prof Cleve Moler at https://blogs.mathworks.com/cleve/2017/09/25/how-far-apart-are-two-random-points-in-a-square/, who credits Presh Talwalker's YouTube channel for posting this puzzle https://youtu.be/i4VqXRRXi68

3.3 Adhesive links between cellulose bundles.

In Section 3.2, we considered that the inter-fibre junctions can be modelled as a 'microfibril-on-microfibril' contact, whereby flat facets of cellulose microfibrils are facing each other. A complication to this model may be introduced when cellulose fibrils bundle together to form a rod-like configuration. We find the majority of junctions formed by bundles exhibit the unwrapping of the twisted motif (Figure 1B & Supplementary Figure S4),resulting in the formation of a flat ribbon-like configuration. The formation of twisted bundles is expected for high aspect ratio fibres due to minimisation of the bending energy. In addition, recent reports suggest that the twist motif is encoded already at the level of individual fibrils and is a result of van der Waals interactions (Kannam, Oehme, Doblin, Gidley, Bacic & Downton, 2017). Although the formation of twisted bundles can be rationalised, the observed untwisting of fibres requires further clarification.

In a number of AFM and SEM images reported for cellulose networks over the last decade (Ding & Liu, 2012; Ding, Zhao & Zeng, 2014; Fanta et al., 2012; Goelzer, Faria-Tischer, Vitorino, Sierakowski & Tischer, 2009; Kafle et al., 2014; Linder, Bergman, Bodin & Gatenholm, 2003; Retegi et al., 2010), we note a phenomenon of fibril 'bulging' in locations where one fibril crosses another. Figure 4 illustrates this effect from our own SEM and AFM observations. In order to minimise the effect of capillary condensation and corresponding capillary forces which may promote fibre deformation in air-dried samples, we have performed imaging on critical point CO_2 dried samples to reduce possible artefacts. Figure 4B depicts a cellulose network with clearly visible bulges that are distributed across the surface and, in some areas, within the depth of the pellicle (as deep as can be probed using AFM). The higher resolution images (Supplementary Figure S4) provide further illustration of twisted fibril bundles, which get split or untwisted around the area of the inter-fibril contact. Due to untwisting of the fibres they produce an apparent 'bulge' that can be clearly visualised in the lower resolution images.

A

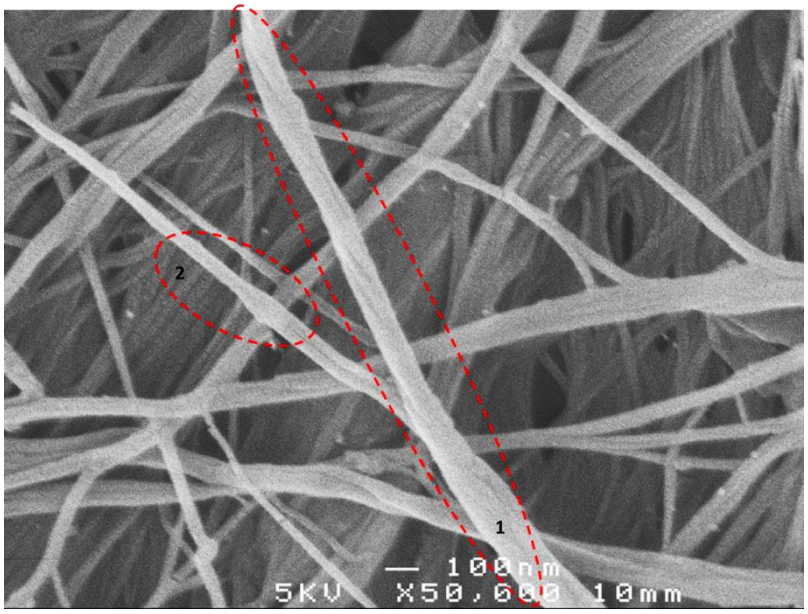

B

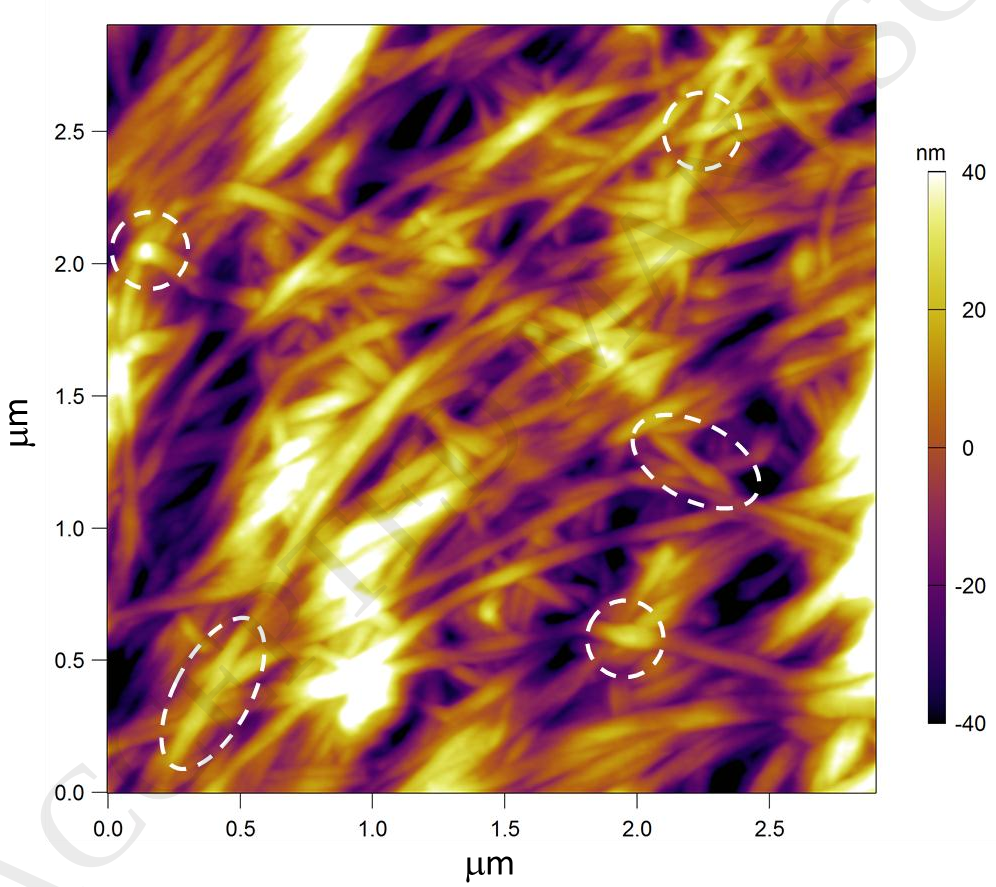

Figure 4. SEM (a) and AFM (B) images of BC networks illustrating the morphology of fibre-fibre contacts. The encircled area '**1**' in A illustrates a twisted fibre. The encircled area '**2**' in A and encircled areas in B illustrate the 'bulging' of fibres in the contact zone.

The AFM and SEM imagess are used to estimate the distribution of the bulging areas and their relative strain, i.e. the ratio of fibre cross-section before and at the junction. Assuming the cellulose fibres have an elastic modulus of 78 GPa (Guhados, Wan & Hutter, 2005), the force required to deform cellulose per single inter-fibre junction to produce a 'bulge' is estimated to be 0.4 mN per junction, which translates to a contact pressure of ~ 6 GPa. Such large pressures are entirely erroneous, as they are at least an order of magnitude larger than the tensile strength of cellulose fibres, ~ 400 MPa (Kafy et al., 2017). This crude estimation suggests that cellulose bundles cannot be treated as a continuous cellulose material, and thus untwisting of bundles becomes a more likely explanation of observed SEM and AFM results. This behaviour has not been reported before, and thus requires further investigation. However, the proposed untwisting is topologically possible during the assembly of the network when bundles have a greater degree of freedom. The effect of 'bulging' is also found in cellulose composites (Supplementary Figure S5), and therefore appears to be a general property characteristic of high aspect ratio bundles.

In the context of our dip-and-drag experiments, this observation has important repercussions in that the interactions between bundles are effectively represented by multiple interactions between elementary cellulose microfibrils. Indeed, if the bundles of fibres have a ribbon like configuration, the junction can be considered as being a superposition of adhesive contacts between elementary fibrils. The significance of this statement is that insights generated in this work can be applicable to other cellulose networks such as plant-derived cell wall preparations where the structure of cellulose bundles can be markedly different compared to that of BC.

4. Cellulose Inter-Fibre Adhesion: The Role of Hemicelluloses

4.1 Results of DnD-LFS on pure BC and on CAX and CXG composite hydrogels

Figure 5 presents typical DnD-LFS lateral force-distance spectra for pure BC hydrogels, as well as CAX and CXG composites. For illustration, the identified peaks in Figure 6 (left panel) are denoted with '*', and the peak height for one of the pull-off events is labelled '*h*' and the corresponding evaluation of the slope is marked with a dash line and labelled 's'. Figures 6A and 6B show histograms of the normalised distributions of the pull-off forces ($F_{\text{pull-off}}$) and the peak slopes (*s*), respectively. The distributions are analysed using the Weibull function, and the measures of central tendency such as mean, median, and mode, as well as skewness, have been extracted and summarised in Table 1.

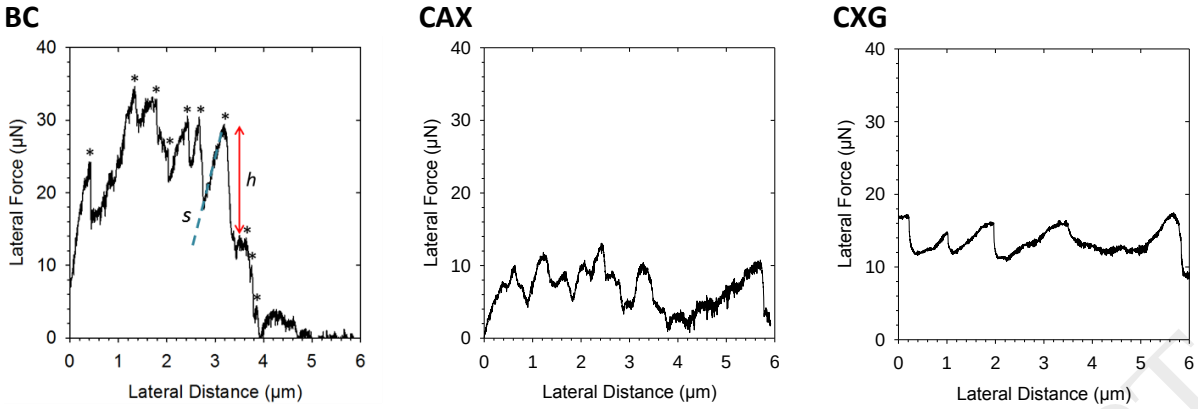

Figure 5. Examples of force-distance curve for pure bacterial cellulose (BC), CAX and CXG fibre networks. The force distance curve shown in the left panel is used as an example force spectrum to illustrate methodological approach. The asterisk symbol denotes the peaks in the curve that represent detachment events at fibre contacts, *h* is an example of the peak height, and *s* is an example of the pre-detachment slope, which is evaluated for each peak event.

Table 1. Parameters of the Weibull distribution fits of the pull-off force ($F_{pull\text{-}off}$) and slope (s) data, and the respective measures of central tendency.

	$F_{pull\text{-}off}$ [μN]					
	λ	*k*	**Mean** $\lambda\Gamma(1+k^{-1})$	**Median** $\lambda\cdot(\ln 2)^{k^{-1}}$	**Mode** $\lambda\cdot(1-k^{-1})^{k^{-1}}$	**Skewness**
BC	0.16	2.5	0.14	0.14	0.13	0.35
CAX	0.21	2.7	0.19	0.18	0.18	0.27
CXG	0.67	3.4	0.60	0.60	0.60	0.06
	***s* [N/m]**					
	λ	*k*	**Mean** $\lambda\Gamma(1+k^{-1})$	**Median** $\lambda\cdot(\ln 2)^{k^{-1}}$	**Mode** $\lambda\cdot(1-k^{-1})^{k^{-1}}$	**Skewness**
BC	2.6	1.5	2.3	2.0	1.3	1.0
CAX	1.5	1.7	1.3	1.2	0.9	0.9
CXG	2.5	1.5	2.3	1.9	1.1	1.1

The distribution in Figure 6A shows that pull-off forces in CXG (0.6 μN) are much larger compared to BC (0.14) and CAX hydrogels (0.19), suggesting stronger adhesive forces. The BC and CAX hydrogels have comparable values of skewness, with CAX hydrogels showing ~35% large pull-off force compared to BC (one way ANOVA, P-Value 0.005). Albeit the distribution for CXG composites is much broader, its skewness parameter is lowest of the three. Overall, the values of skewness are low, suggesting that distributions for all three types of hydrogels are close to the normal.

The distribution of the initial linear slopes, *s*, are found to be more skewed (Figure 6B); the skewness parameter for all three hydrogels is found to be ~1. The narrowest distribution is observed for CAX hydrogels. The values of the initial linear slope suggest that *s* is markedly larger compared to ∇F_{CZM} (~ 0.4 N/m) estimated based on the cohesion zone model (CZM). Therefore, *s* reflects the micromechanics of cellulose network and can be interpreted as an effective spring constant for the localised fibre network. The results suggest that BC and CXG networks have almost identical micromechanics, whereas CAX hydrogels are somewhat weaker. That being said, the mode values of *s* are found to be very similar between all three hydrogels, suggesting that mechanical properties of fibre networks are comparable. To further support this statement, SEM images of the cellulose, CAX, and CXG networks are shown in Supplementary Figure S6. Whilst some differences are observed, one can conclude that hemicelluloses have no substantial effect on the thickness of bundles and the overall topology of the network.

In order to explore the influence of network micromechanics on the measured values of the pull-off force, the pull-off force data are plotted against the initial linear slope for each individual detachment event as shown in Figure 7. The purpose of this analysis is twofold: first, we test prediction of the CZM model that network configuration has little effect on the measured pull-off force; and, second, we validate the principle of DnD-LFS technique, which relies on the force balance between fibre deformation and fibre adhesion/detachment. The results shown in Figure 7 demonstrate that the values of pull-off force weakly correlate with the corresponding value of the initial linear slope. For convenience, we used power law regression to find the values of the power law exponent, which is found to be in the range from 0.1 for CXG and CAX hydrogels to 0.15 for pure BC. The spread in the values of the slope, which range anywhere from 0.1 to 10 N/m, suggest we probe a vastly diverse ensemble of network configurations. Some configuration may be dense and stiff, while others may comprise lower number of fibres and, consequently, are weaker. The very weak dependency of the pull-off force on the slope suggests that the conclusions from the CZM modelling are adequate, and hence eq 5 provides a good first-order approximation of the adhesive behaviour of fibre-fibre contacts. Secondly, the observed weak dependence does indicate that 'dipping' the AFM tip into a denser network and 'dragging' a greater portion of entangled fibres increases our chances of rupturing stronger adhesive contacts that represent the 'tougher' end of the distribution across the ensemble, as illustrated in Figure 7 (inset, bottom panel).

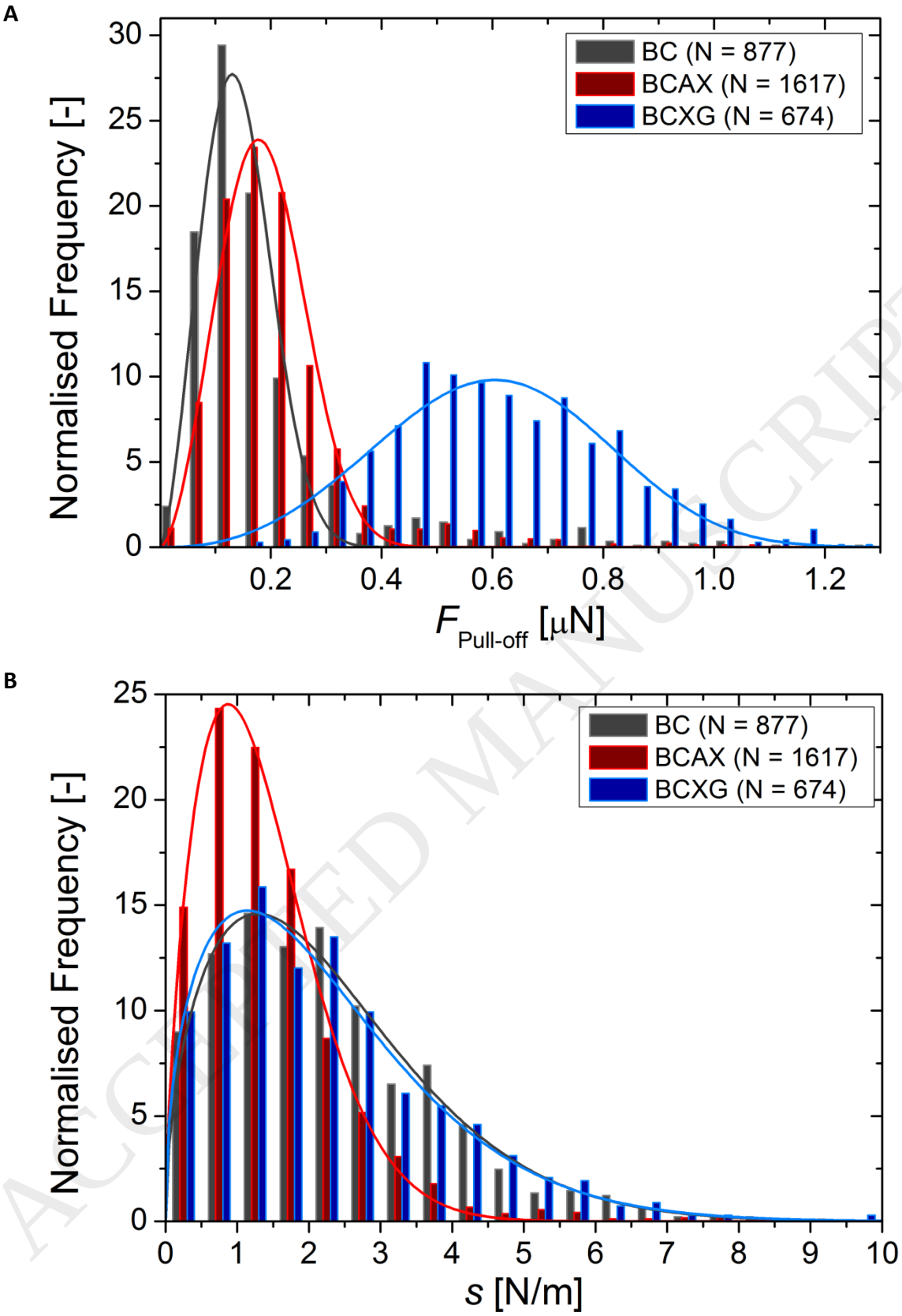

Figure 6. Normalised histograms of $F_{pull-off}$ (B) and *s* (C) distributions for a complete data set measured on BC (N=877), CAX (N=1617) and CXG (N=674). Solid lines represent the best fit using the Weibull function.

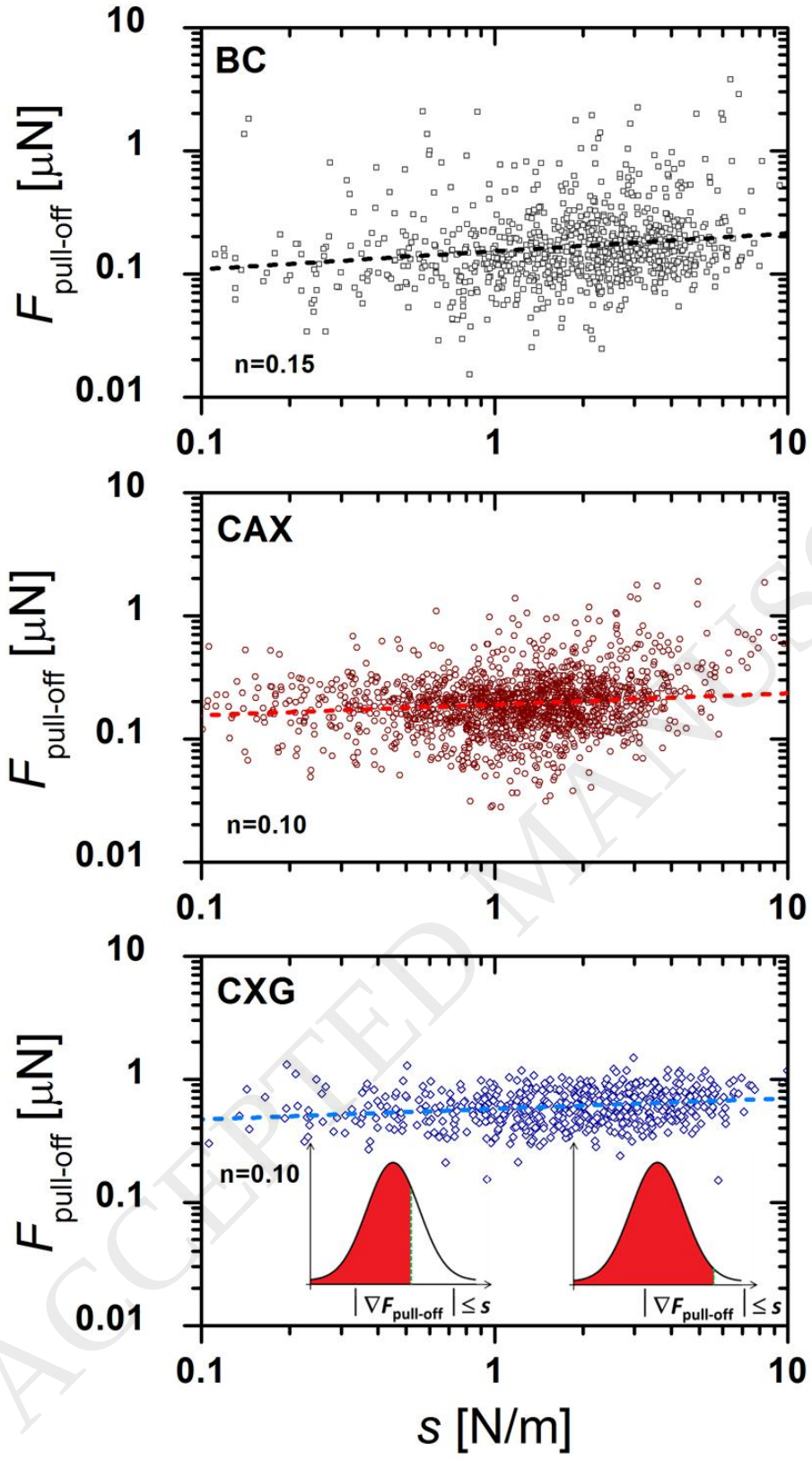

Figure 7. The plots of correlation between $F_{pull-off}$ and s for BC (N=877), CAX (N=1617) and CXG (N=674). Dash lines represent the power law regression fits. The values of power law exponent, n, are found to be of the order of 0.10 – 0.15. The inset in the bottom panel illustrates that with the increasing of the initial linear slope, s, we probe a progressively larger area of the distribution of pull-off forces.

The mean values of $F_{pull\text{-}off}$ are substituted in eq 5 to calculate the values of the adhesion energy per unit area ($\Delta\gamma$) and the strength of cellulose fibre-fibre contact (K_0). In all calculations, we use the ensemble average bundle width D_B = 48 nm and the separation distance δ = 0.3 nm. Further, the values of K_0 as well as $\langle b \rangle$ = 1.47 are substituted into eq 3 to yield the values of ∇F_{CZM} ([c]). All obtained values are summarized in Table 2. As already deduced from the distribution of pull-off forces, the fibre-fibre adhesion in CXG network is 4.3 times stronger compared to BC. The CAX and BC networks are comparable; still, the contacts in CAX network are ~30% more adhesive compared to BC.

Table 2. Parameters of adhesive contact of pure BC, and CAX and CXG composite hydrogels calculated from the mean values of the pull-off force using eq 5.

	BC	**CAX**	**CXG**
K_0 [MPa]	60	80	260
$\Delta\gamma$ [mJ/m^2]	18	24	79
∇F_{CZM} [N/m]	0.23	0.27	0.48
d_I [Å]	7.8	6.8	3.7

The values of $\Delta\gamma$ for cellulose hydrogels are consistent with those estimated for the contacts dominated by hydrogen bond interactions. This result shows that in nano-cellulose assemblies the interaction between cellulose fibres is related to hydrogen bonding, and the contribution from the van der Waals forces is small. Using $\Delta\gamma$ values in Table 2 we have estimated the number of hydrogen bonds per unit area assuming the energy of hydrogen bonding in water is 6.6 kJ/mol (Sheu, Yang, Selzle & Schlag, 2003) (Table 2). The results suggest that the average distance between hydrogen bonds for BC and CAX is approximately twice larger compared to 4.5 Å estimated based on the distance between the layers along the polymerisation axis of cellulose microfibrils (Martinez-Sanz, Mikkelsen, Flanagan, Gidley & Gilbert, 2016; Martinez-Sanz et al., 2016). In CXG hydrogels, the spacing is smaller, 3.7 Å, which can be associated with the increased density of hydrogen bonds due to presence of xyloglucan.

4.2 Discussion on the role of XG and AX in cellulose fibre-fibre interactions

The use of BC as a model of primary plant cell wall (PCW) is frequently scrutinised. Indeed, BC and cellulose network in primary PCW of higher plants differ in many regards. One of the key differences is topology of entanglements (Park & Cosgrove, 2012b) that may influence the mechanical response of BC-based materials under conditions of bulk

[c] Based on the SEM images of pure BC, CAX, and CXG networks shown in Supplementary Figure S6, we conclude that all three types of networks have similar topology. Therefore, the geometric argument (Figure 3B, inset) used to estimate parameter $\langle b \rangle$ is applicable for all three types of cellulose hydrogels.

mechanical tests such as uniaxial extension (Mikkelsen, Flanagan, Wilson, Bacic & Gidley, 2015). Gu and Catchmark (2014) proposed that during the biosynthesis of BC, the adsorption of XG onto the cellulose surface reduces the number of network entanglements. On the macroscale, this reduction may result in the reduced modulus of the network. Another possible mechanism is that XG may promote lubrication between cellulose fibrils and bundles, which may contribute to the reduced macroscopic stiffness of CXG composite networks. This hypothesis would be consistent with the data on the static friction between two bacterial cellulose hydrogel surfaces, which is driven by the adhesion between individual cellulose fibres at the interface (Dolan, Yakubov, Bonilla, Lopez-Sanchez & Stokes, 2017). The static friction between pairs of cellulose hydrogels is shown to be reduced by approximately half in the presence of XG.

The use of DnD-LFS strips down several levels of complexity and provides, like never before, a window to probe single cellulose-cellulose junctions on a fundamental physical level. The results from the DnD-LFS technique confirm that the key interaction that holds cellulose network assemblies together is hydrogen bonding. Furthermore, the results strongly suggest that XG has a direct effect on the interaction between cellulose fibres by increasing the adhesion energy via promoting formation of hydrogen bonds. These results provide strong evidence to support the Park and Cosgrove model of primary PCWs (Park & Cosgrove, 2012b), where the presence of xyloglucan confined within cellulose-cellulose junctions is a key load-bearing element of the cellulose fibre assembly (schematically shown in Figure 8A). The mechanism by which XG promotes hydrogen bonding may well be association with the ability of XG to specifically adsorb on the surface of cellulose fibrils; this effect is well-attested in the literature (Dammak et al., 2015; Gu & Catchmark, 2014; Hanus & Mazeau, 2006; Lima, Loh & Buckeridge, 2004; Mysliwiec, Chylinska, Szymanska-Chargot, Chibowski & Zdunek, 2016; Park & Cosgrove, 2015; Villares, Moreau, Dammak, Capron & Cathala, 2015; Whitney, Brigham, Darke, Reid & Gidley, 1995; Zhang, Brumer, Agren & Tu, 2011; Zhao, Crespi, Kubicki, Cosgrove & Zhong, 2014; Zykwinska, Thibault & Ralet, 2008). Importantly, the adsorption process is governed by hydrogen bonding between xyloglucan and cellulose, i.e. the same interaction that is responsible for adhesion (Hanus & Mazeau, 2006; Zhang, Brumer, Agren & Tu, 2011).

The behaviour of fibre-fibre contacts in CAX composites appears to be similar to pure BC, although we observe a notable increase in K_0 and $\Delta\gamma$ in CAX composites. We propose that AX influences cellulose-cellulose contacts via hydrogen bonding. However, unlike XG, AX shows weaker and less specific binding to cellulose (Martinez-Sanz, Mikkelsen, Flanagan, Gidley & Gilbert, 2017; Mikkelsen, Flanagan, Wilson, Bacic & Gidley, 2015). Due to weaker binding, the contribution of AX molecules to the adhesion is attenuated as illustrated in Figure 8B. In addition, due to non-specific nature of binding, AX can adapt multiple configurations within the inter-fibre contact zone, and may not be necessarily sandwiched between cellulose fibrils, as it was postulated for the case of XG.

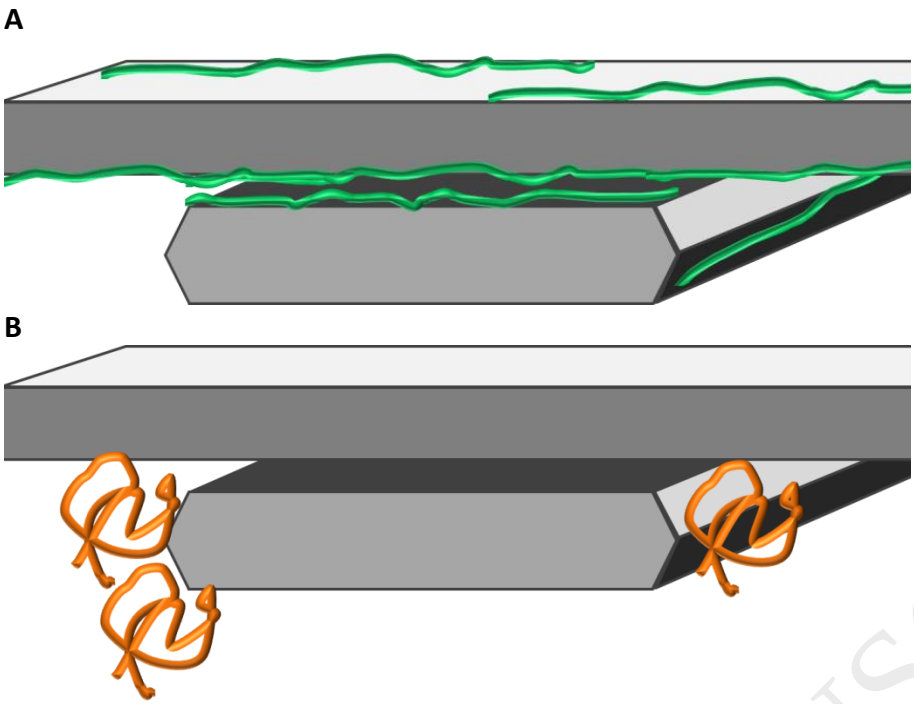

Figure 8. Illustration of proposed configuration of cellulose-cellulose inter-fibre contact mediated by hemicellulose. (A) A fibre-fibre contact modulated by XG molecules sandwiched between cellulose fibrils. (B) A possible contact configuration for CAX composites, which may include tethered AX chains that contribute to the adhesive force between cellulose fibres.

For both AX and XG, the energy per unit area increases compared to pure bacterial cellulose, suggesting that these polysaccharides have a strong effect on fibre-fibre adhesion. These findings are instrumental to support a number of emerging models of cellulose networks, including plant cell walls (Cosgrove, 2014). The emerging school of thought postulates that different types of contacts may co-exist within the network and the unique properties of such a network stem from the diversity in mechanical properties of fibre-fibre contacts, which are required to be of tuneable strength to enable wall extensions and cell/tissue growth (Cosgrove, 2014).

5 Conclusions

The DnD-LFS technique enables the probing of molecular interactive forces between cellulose fibres in cellulose composite hydrogels. We interpret the measured peaks in lateral force-distance curves as representing fibre-fibre detachment events. Simulation of fibre-fibre detachment is used to perform a sensitivity analysis on predicted measurements with system variables (contact strength and network structure), which found that the pull-off force is related to the adhesion energy between fibres. The DnD-LFS results show that the adhesive contacts are dominated by hydrogen bonding, and the presence of XG or AX in the cellulose network increases the adhesive forces between fibres by a factor of 4.3 and 1.3,

respectively. It is hypothesised that XG boosts adhesion by increasing the density of hydrogen bonding, which, we hypothesise, may be due to adsorption of XG on the surface of cellulose fibrils.

These findings are consistent with the revised model of primary plant cell walls (Park & Cosgrove, 2012b), where cellulose-cellulose junctions assembled in the presence of xyloglucan confined between fibrils act as a key load-bearing element of the cellulose network. These findings give fresh insights into the way the mechanical properties of cellulose networks are controlled through the composition and assembly of cellulose-hemicellulose hybrid networks.

Acknowledgements

The authors gratefully acknowledge Ms Dongjie Wang for acquiring SEM images used in Figure 4 and Supplementary Figure S5. Dr. Patricia Lopez-Sanchez is gratefully acknowledged for providing SEM images used in Supplementary Figure S6. This work was performed at the Queensland Node of the Australian National Fabrication Facility (ANFF-Q), a company established under the National Collaborative Research Infrastructure Strategy to provide nano- and microfabrication facilities for Australia's researchers. G.K.D. and B.C. acknowledge financial support of the UQ Postgraduate Research Scholarship. J.R.S. and G.E.Y. acknowledge financial support of the Australian Research Council Discovery Project (DP150104147). The research is supported by an Australian Research Council Centre of Excellence in Plant Cell Walls (CE110001007).

References

Andersson, S. R., & Rasmuson, A. (1997). Dry and wet friction of single pulp and synthetic fibres. *Journal of Pulp and Paper Science, 23*(1), J5-J11.

Baba, K., Sone, Y., Misaki, A., & Hayashi, T. (1994). Localization of xyloglucan in the macromolecular complex composed of xyloglucan and cellulose in pea stems. *Plant and Cell Physiology, 35*(3), 439-444.

Bonilla, M. R., Lopez-Sanchez, P., Gidley, M. J., & Stokes, J. R. (2016). Micromechanical model of biphasic biomaterials with internal adhesion: Application to nanocellulose hydrogel composites. *Acta Biomaterialia, 29*, 149-160.

Carambassis, A., & Rutland, M. W. (1999). Interactions of cellulose surfaces: Effect of electrolyte. *Langmuir, 15*(17), 5584-5590.

Carbone, G., & Pierro, E. (2013). A review of adhesion mechanisms of mushroom-shaped microstructured adhesives. *Meccanica, 48*(8), 1819-1833.

Chanliaud, E., Burrows, K. M., Jeronimidis, G., & Gidley, M. J. (2002). Mechanical properties of primary plant cell wall analogues. *Planta, 215*(6), 989-996.

Chen, S. Q., Mikkelsen, D., Lopez-Sanchez, P., Wang, D. J., Martinez-Sanz, M., Gilbert, E. P., Flanagan, B. M., & Gidley, M. J. (2017). Characterisation of bacterial cellulose from diverse Komagataeibacter strains and their application to construct plant cell wall analogues. *Cellulose, 24*(3), 1211-1226.

Cosgrove, D. J. (2014). Re-constructing our models of cellulose and primary cell wall assembly. *Current Opinion in Plant Biology, 22*, 122-131.

Dammak, A., Quemener, B., Bonnin, E., Alvarado, C., Bouchet, B., Villares, A., Moreau, C., & Cathala, B. (2015). Exploring Architecture of Xyloglucan Cellulose Nanocrystal Complexes through Enzyme Susceptibility at Different Adsorption Regimes. *Biomacromolecules, 16*(2), 589-596.

de Oliveira Barud, H. G., da Silva, R. R., da Silva Barud, H., Tercjak, A., Gutierrez, J., Lustri, W. R., de Oliveira, O. B., & Ribeiro, S. J. L. (2016). A multipurpose natural and renewable polymer in medical applications: Bacterial cellulose. *Carbohydrate Polymers, 153*, 406-420.

Ding, S.-Y., & Liu, Y.-S. (2012). Imaging cellulose using atomic force microscopy. *Methods in molecular biology (Clifton, N.J.), 908*, 23-30.

Ding, S.-Y., Zhao, S., & Zeng, Y. (2014). Size, shape, and arrangement of native cellulose fibrils in maize cell walls. *Cellulose, 21*(2), 863-871.

Dolan, G. K. (2017). Bio-tribology of plant cell walls: measuring the interactive forces between cell wall components. PhD Thesis. *School of Chemical Engineering* (p. 262). Brisbane, Australia: The University of Queensland.

Dolan, G. K., Yakubov, G. E., Bonilla, M. R., Lopez-Sanchez, P., & Stokes, J. R. (2017). Friction, lubrication, and in situ mechanics of poroelastic cellulose hydrogels. *Soft Matter, 13*(19), 3592-3601.

Dolan, G. K., Yakubov, G. E., Greene, G. W., Amiralian, N., Annamalai, P. K., Martin, D. J., & Stokes, J. R. (2016). Dip-and-Drag Lateral Force Spectroscopy for Measuring Adhesive Forces between Nanofibers. *Langmuir, 32*(50), 13340-13348.

Dolan, G. K., Yakubov, G. E., & Stokes, J. R. (2018). Bio-Tribology and Bio-Lubrication of Plant Cell Walls. In J. A. Roberts (Ed.). *Annual Plant Reviews online*: John Wiley & Sons.

Fanta, S. W., Vanderlinden, W., Abera, M. K., Verboven, P., Karki, R., Quang Tri, H., De Feyter, S., Carmeliet, J., & Nicolai, B. M. (2012). Water transport properties of artificial cell walls. *Journal of Food Engineering, 108*(3), 393-402.

Fernandes, A. N., Thomas, L. H., Altaner, C. M., Callow, P., Forsyth, V. T., Apperley, D. C., Kennedy, C. J., & Jarvis, M. C. (2011). Nanostructure of cellulose microfibrils in spruce wood. *Proceedings of the National Academy of Sciences of the United States of America, 108*(47), E1195-E1203.

Finkenstadt, V. L., Hendrixson, T. L., & Millane, R. P. (1995). Models of xyloglucan binding to cellulose microfibrils. *Journal of Carbohydrate Chemistry, 14*(4-5), 601-611.

Gartaula, G., Dhital, S., Netzel, G., Flanagan, B. M., Yakubov, G. E., Beahan, C. T., Collins, H. M., Burton, R. A., Bacic, A., & Gidley, M. J. (2018). Quantitative structural organisation model for wheat endosperm cell walls: Cellulose as an important constituent. *Carbohydrate Polymers, 196*, 199-208.

Goelzer, F. D. E., Faria-Tischer, P. C. S., Vitorino, J. C., Sierakowski, M.-R., & Tischer, C. A. (2009). Production and characterization of nanospheres of bacterial cellulose from Acetobacter xylinum from processed rice bark. *Materials Science & Engineering C-Biomimetic and Supramolecular Systems, 29*(2), 546-551.
Green, C. P., Lioe, H., Cleveland, J. P., Proksch, R., Mulvaney, P., & Sader, J. E. (2004). Normal and torsional spring constants of atomic force microscope cantilevers. *Review of Scientific Instruments, 75*(6), 1988-1996.
Gu, J., & Catchmark, J. M. (2014). Roles of xyloglucan and pectin on the mechanical properties of bacterial cellulose composite films. *Cellulose, 21*(1), 275-289.
Guhados, G., Wan, W. K., & Hutter, J. L. (2005). Measurement of the elastic modulus of single bacterial cellulose fibers using atomic force microscopy. *Langmuir, 21*(14), 6642-6646.
Hanus, J., & Mazeau, K. (2006). The xyloglucan-cellulose assembly at the atomic scale. *Biopolymers, 82*(1), 59-73.
Hrmova, M., Farkas, V., Lahnstein, J., & Fincher, G. B. (2007). A barley xyloglucan xyloglucosyl transferase covalently links xyloglucan, cellulosic substrates, and (1,3;1,4)-beta-D-glucans. *Journal of Biological Chemistry, 282*(17), 12951-12962.
Huang, F., Li, K. C., & Kulachenko, A. (2009). Measurement of interfiber friction force for pulp fibers by atomic force microscopy. *Journal of Materials Science, 44*(14), 3770-3776.
Johnson, K. L., Gidley, M. J., Bacic, A., & Doblin, M. S. (2018). Cell wall biomechanics: a tractable challenge in manipulating plant cell walls 'fit for purpose'! *Current Opinion in Biotechnology, 49*, 163-171.
Kafle, K., Xi, X. N., Lee, C. M., Tittmann, B. R., Cosgrove, D. J., Park, Y. B., & Kim, S. H. (2014). Cellulose microfibril orientation in onion (Allium cepa L.) epidermis studied by atomic force microscopy (AFM) and vibrational sum frequency generation (SFG) spectroscopy. *Cellulose, 21*(2), 1075-1086.
Kafy, A., Kim, H. C., Zhai, L. D., Kim, J. W., Van Hai, L., Kang, T. J., & Kim, J. (2017). Cellulose long fibers fabricated from cellulose nanofibers and its strong and tough characteristics. *Scientific Reports, 7*.
Kannam, S. K., Oehme, D. P., Doblin, M. S., Gidley, M. J., Bacic, A., & Downton, M. T. (2017). Hydrogen bonds and twist in cellulose microfibrils. *Carbohydrate Polymers, 175*(Supplement C), 433-439.
Keegstra, K., Talmadge, K. W., Bauer, W. D., & Albershe.P. (1973). Structure of plant-cell walls. 3. Model of walls of suspension-cultured sycamore cells based on interconnections of macromolecular components. *Plant Physiology, 51*(1), 188-196.
Kulasinski, K., Keten, S., Churakov, S. V., Derome, D., & Carmeliet, J. (2014). A comparative molecular dynamics study of crystalline, paracrystalline and amorphous states of cellulose. *Cellulose, 21*(3), 1103-1116.
Lima, D. U., Loh, W., & Buckeridge, M. S. (2004). Xyloglucan-cellulose interaction depends on the sidechains and molecular weight of xyloglucan. *Plant Physiology and Biochemistry, 42*(5), 389-394.
Linder, A., Bergman, R., Bodin, A., & Gatenholm, P. (2003). Mechanism of assembly of xylan onto cellulose surfaces. *Langmuir, 19*(12), 5072-5077.
Lopez-Sanchez, P., Cersosimo, J., Wang, D., Flanagan, B., Stokes, J. R., & Gidley, M. J. (2015). Poroelastic Mechanical Effects of Hemicelluloses on Cellulosic Hydrogels under Compression. *PLOS ONE, 10*(3), e0122132.
Lopez-Sanchez, P., Martinez-Sanz, M., Bonilla, M. R., Wang, D., Gilbert, E. P., Stokes, J. R., & Gidley, M. J. (2017). Cellulose-pectin composite hydrogels: Intermolecular interactions and material properties depend on order of assembly. *Carbohydrate Polymers, 162*, 71-81.
Lopez-Sanchez, P., Martinez-Sanz, M., Bonilla, M. R., Wang, D. J., Walsh, C. T., Gilbert, E. P., Stokes, J. R., & Gidley, M. J. (2016). Pectin impacts cellulose fibre architecture and hydrogel mechanics in the absence of calcium. *Carbohydrate Polymers, 153*, 236-245.
Lopez-Sanchez, P., Rincon, M., Wang, D., Brulhart, S., Stokes, J. R., & Gidley, M. J. (2014). Micromechanics and Poroelasticity of Hydrated Cellulose Networks. *Biomacromolecules, 15*(6), 2274-2284.

Lv, X. G., Yang, J. X., Feng, C., Li, Z., Chen, S. Y., Xie, M. K., Huang, J. W., Li, H. B., Wang, H. P., & Xu, Y. M. (2016). Bacterial Cellulose-Based Biomimetic Nanofibrous Scaffold with Muscle Cells for Hollow Organ Tissue Engineering. *Acs Biomaterials Science & Engineering, 2*(1), 19-29.
Martinez-Sanz, M., Gidley, M. J., & Gilbert, E. P. (2015). Application of X-ray and neutron small angle scattering techniques to study the hierarchical structure of plant cell walls: A review. *Carbohydrate Polymers, 125*, 120-134.
Martinez-Sanz, M., Gidley, M. J., & Gilbert, E. P. (2016). Hierarchical architecture of bacterial cellulose and composite plant cell wall polysaccharide hydrogels using small angle neutron scattering. *Soft Matter, 12*(5), 1534-1549.
Martinez-Sanz, M., Lopez-Sanchez, P., Gidley, M. J., & Gilbert, E. P. (2015). Evidence for differential interaction mechanism of plant cell wall matrix polysaccharides in hierarchically-structured bacterial cellulose. *Cellulose, 22*(3), 1541-1563.
Martinez-Sanz, M., Mikkelsen, D., Flanagan, B., Gidley, M. J., & Gilbert, E. P. (2016). Multi-scale model for the hierarchical architecture of native cellulose hydrogels. *Carbohydrate Polymers, 147*, 542-555.
Martinez-Sanz, M., Mikkelsen, D., Flanagan, B. M., Gidley, M. J., & Gilbert, E. P. (2017). Multi-scale characterisation of deuterated cellulose composite hydrogels reveals evidence for different interaction mechanisms with arabinoxylan, mixed-linkage glucan and xyloglucan. *Polymer, 124*, 1-11.
Martinez-Sanz, M., Mikkelsen, D., Flanagan, B. M., Rehm, C., de Campo, L., Gidley, M. J., & Gilbert, E. P. (2016). Investigation of the micro- and nano-scale architecture of cellulose hydrogels with plant cell wall polysaccharides: A combined USANS/SANS study. *Polymer, 105*, 449-460.
McNeil, M., Albersheim, P., Taiz, L., & Jones, R. L. (1975). Structure of plant-cell walls. 7. Barley aleurone cells. *Plant Physiology, 55*(1), 64-68.
Mikkelsen, D., Flanagan, B. M., Wilson, S. M., Bacic, A., & Gidley, M. J. (2015). Interactions of Arabinoxylan and (1,3)(1,4)-beta-Glucan with Cellulose Networks. *Biomacromolecules, 16*(4), 1232-1239.
Mikkelsen, D., & Gidley, M. J. (2011). Formation of Cellulose-Based Composites with Hemicelluloses and Pectins Using Gluconacetobacter Fermentation. In Z. A. Popper (Ed.). *Plant Cell Wall: Methods and Protocols* (Vol. 715, pp. 197-208). Totowa: Humana Press Inc.
Mysliwiec, D., Chylinska, M., Szymanska-Chargot, M., Chibowski, S., & Zdunek, A. (2016). Revision of adsorption models of xyloglucan on microcrystalline cellulose. *Cellulose, 23*(5), 2819-2829.
Nigmatullin, R., Lovitt, R., Wright, C., Linder, M., Nakari-Setala, T., & Gama, A. (2004). Atomic force microscopy study of cellulose surface interaction controlled by cellulose binding domains. *Colloids and Surfaces B-Biointerfaces, 35*(2), 125-135.
Notley, S. M., Eriksson, M., Wagberg, L., Beck, S., & Gray, D. G. (2006). Surface forces measurements of spin-coated cellulose thin films with different crystallinity. *Langmuir, 22*(7), 3154-3160.
Notley, S. M., Pettersson, B., & Wågberg, L. (2004). Direct Measurement of Attractive van der Waals' Forces between Regenerated Cellulose Surfaces in an Aqueous Environment. *Journal of the American Chemical Society, 126*(43), 13930-13931.
Oehme, D. P., Doblin, M. S., Wagner, J., Bacic, A., Downton, M. T., & Gidley, M. J. (2015). Gaining insight into cell wall cellulose macrofibril organisation by simulating microfibril adsorption. *Cellulose, 22*(6), 3501-3520.
Oehme, D. P., Downton, M. T., Doblin, M. S., Wagner, J., Gidley, M. J., & Bacic, A. (2015). Unique Aspects of the Structure and Dynamics of Elementary I beta Cellulose Microfibrils Revealed by Computational Simulations. *Plant Physiology, 168*(1), 3-U654.
Park, K., & Paulino, G. H. (2011). Cohesive Zone Models: A Critical Review of Traction-Separation Relationships Across Fracture Surfaces. *Applied Mechanics Reviews, 64*(6).
Park, Y. B., & Cosgrove, D. J. (2012a). Changes in Cell Wall Biomechanical Properties in the Xyloglucan-Deficient xxt1/xxt2 Mutant of Arabidopsis. *Plant Physiology, 158*(1), 465-475.

Park, Y. B., & Cosgrove, D. J. (2012b). A Revised Architecture of Primary Cell Walls Based on Biomechanical Changes Induced by Substrate-Specific Endoglucanases. *Plant Physiology, 158*(4), 1933-1943.
Park, Y. B., & Cosgrove, D. J. (2015). Xyloglucan and its Interactions with Other Components of the Growing Cell Wall. *Plant and Cell Physiology, 56*(2), 180-194.
Raviv, U., Laurat, P., & Klein, J. (2001). Fluidity of water confined to subnanometre films. *Nature, 413*(6851), 51-54.
Retegi, A., Gabilondo, N., Pena, C., Zuluaga, R., Castro, C., Ganan, P., de la Caba, K., & Mondragon, I. (2010). Bacterial cellulose films with controlled microstructure-mechanical property relationships. *Cellulose, 17*(3), 661-669.
Sheu, S. Y., Yang, D. Y., Selzle, H. L., & Schlag, E. W. (2003). Energetics of hydrogen bonds in peptides. *Proceedings of the National Academy of Sciences of the United States of America, 100*(22), 12683-12687.
Shi, Z. J., Zhang, Y., Phillips, G. O., & Yang, G. (2014). Utilization of bacterial cellulose in food. *Food Hydrocolloids, 35*, 539-545.
Stiernstedt, J., Brumer, H., III, Zhou, Q., Teeri, T. T., & Rutland, M. W. (2006). Friction between cellulose surfaces and effect of xyloglucan adsorption. *Biomacromolecules, 7*(7), 2147-2153.
Stiernstedt, J., Nordgren, N., Wagberg, L., Brumer, H., Gray, D. G., & Rutland, M. W. (2006). Friction and forces between cellulose model surfaces: A comparison. *Journal of Colloid and Interface Science, 303*(1), 117-123.
Villares, A., Moreau, C., Dammak, A., Capron, I., & Cathala, B. (2015). Kinetic aspects of the adsorption of xyloglucan onto cellulose nanocrystals. *Soft Matter, 11*(32), 6472-6481.
Wagner, K., Cheng, P., & Vezenov, D. (2011). Noncontact Method for Calibration of Lateral Forces in Scanning Force Microscopy. *Langmuir, 27*(8), 4635-4644.
Whitney, S. E. C., Brigham, J. E., Darke, A. H., Reid, J. S. G., & Gidley, M. J. (1995). In-vitro assembly of cellulose/xyloglucan networks - ultrastructural and molecular aspects. *Plant Journal, 8*(4), 491-504.
Whitney, S. E. C., Gothard, M. G. E., Mitchell, J. T., & Gidley, M. J. (1999). Roles of cellulose and xyloglucan in determining the mechanical properties of primary plant cell walls. *Plant Physiology, 121*(2), 657-663.
Yakubov, G. E., Bonilla, M. R., Chen, H. Y., Doblin, M. S., Bacic, A., Gidley, M. J., & Stokes, J. R. (2016). Mapping nano-scale mechanical heterogeneity of primary plant cell walls. *Journal of Experimental Botany, 67*(9), 2799-2816.
Yakubov, G. E., Macakova, L., Wilson, S., Windust, J. H. C., & Stokes, J. R. (2015). Aqueous lubrication by fractionated salivary proteins: Synergistic interaction of mucin polymer brush with low molecular weight macromolecules. *Tribology International, 89*, 34-45.
Yang, J., & Li, J. (2018). Self-assembled cellulose materials for biomedicine: A review. *Carbohydrate Polymers, 181*, 264-274.
Zauscher, S., & Klingenberg, D. J. (2001). Friction between cellulose surfaces measured with colloidal probe microscopy. *Colloids and Surfaces a-Physicochemical and Engineering Aspects, 178*(1-3), 213-229.
Zhang, Q., Brumer, H., Agren, H., & Tu, Y. Q. (2011). The adsorption of xyloglucan on cellulose: effects of explicit water and side chain variation. *Carbohydrate Research, 346*(16), 2595-2602.
Zhang, T., Mahgsoudy-Louyeh, S., Tittmann, B., & Cosgrove, D. J. (2014). Visualization of the nanoscale pattern of recently-deposited cellulose microfibrils and matrix materials in never-dried primary walls of the onion epidermis. *Cellulose, 21*(2), 853-862.
Zhang, T., Zheng, Y. Z., & Cosgrove, D. J. (2016). Spatial organization of cellulose microfibrils and matrix polysaccharides in primary plant cell walls as imaged by multichannel atomic force microscopy. *Plant Journal, 85*(2), 179-192.
Zhao, B., & Kwon, H. J. (2011). Adhesion of Polymers in Paper Products from the Macroscopic to Molecular Level - An Overview. *Journal of Adhesion Science and Technology, 25*(6-7), 557-579.

Zhao, Z., Crespi, V. H., Kubicki, J. D., Cosgrove, D. J., & Zhong, L. H. (2014). Molecular dynamics simulation study of xyloglucan adsorption on cellulose surfaces: effects of surface hydrophobicity and side-chain variation. *Cellulose, 21*(2), 1025-1039.
Zykwinska, A., Thibault, J. F., & Ralet, M. C. (2008). Modelling of xyloglucan, pectins and pectic side chains binding onto cellulose microfibrils. *Carbohydrate Polymers, 74*(1), 23-30.
Zykwinska, A. W., Ralet, M. C. J., Garnier, C. D., & Thibault, J. F. J. (2005). Evidence for in vitro binding of pectin side chains to cellulose. *Plant Physiology, 139*(1), 397-407.